LBL-12678

BRAGG CURVE SPECTROSCOPY

Invited Talk
INS International Conference on
Radiation Detectors, Tokyo, Japan
March 23-28, 1981

C. R. Gruhn

May 1981

Nuclear Science Division
Lawrence Berkeley Laboratory
University of California
Berkeley, CA 94720

This work was supported by the Director, Office of Energy Research, Division of Nuclear Physics of the Office of High Energy and Nuclear Physics and by Nuclear Sciences of the Basic Energy Sciences Program of the U.S. Department of Energy under Contract W-7405-ENG-48.

BRAGG CURVE SPECTROSCOPY

C. R. Gruhn

Nuclear Science Division
Lawrence Berkeley Laboratory
University of California
Berkeley, CA 94720

I. Introduction

We present in this paper an alternative utilization of the gaseous ionization chamber in the detection of energetic heavy ions, which we call Bragg Curve Spectroscopy (BCS). Conceptually, BCS involves using the maximum data available from the Bragg curve of the stopping heavy ion (HI) for purposes of identifying the particle and measuring its energy. A detector has been designed that measures the Bragg curve with high precision. From the Bragg curve we determine the range from the length of the track, the total energy from the integral of the specific ionization over the track, the dE/dx from the specific ionization at the beginning of the track, and the Bragg peak from the maximum of the specific ionization of the HI. This last signal measures the atomic number, Z, of the HI unambiguously.

Several advantages are realized in this type of HI detector. The detector is relatively insensitive to radiation effects. Large solid angles are easily achieved. The resolution for identifying particles is intrinsically high because all the measurements are made in one medium eliminating window or dead layer effects. Particle identification can in principle be achieved over a large dynamic range in energies and particles.

This paper presents some of our first experiences with the BCS concept. We shall not compare this detector with alternative concepts.

We shall emphasize the interpretation of our results and point out some of the remaining problems to be explored.

II. Detector Design

The detector design is an ionization chamber with a Frisch grid to cathode distance longer than the range of the particles to be stopped. The anode to grid spacing is shorter than the lowest range HI of interest. The particles enter through the cathode and leave an ionization track parallel to the electric field. The electrons along the track are drifted through the grid and viewed as an anode current. The anode current as a function of time is proportional to the specific ionization along the track. The more important parameters of the detector used in this paper are presented in Table I.

We have used conventional NIM electronics to realize the results presented in this paper. The anode signal is viewed with a charge sensitive preamplifier. The preamplifier is connected in parallel to the electronics which yields the energy, the Bragg peak, the range, and dE/dx of particle. The energy signal is obtained using a shaping amplifier with a time constant long compared to the current pulse length (8μs). The Bragg peak signal is obtained using a shaping amplifier with a time constant approximately equal to the electron transit time between the grid and the anode. This signal when viewed on the oscilloscope should be representative of the Bragg curve. It is also useful as a diagnostic of what is happening to the electrons as a function of position in the detector. This shaping amplifier is followed by a peak stretcher that yields the Bragg peak signal ready to be digitized. The

range or length of the track is measured by delay line shaping the Bragg peak signal. The Bragg peak signal is used to start a TAC. The negative (and trailing) portion of the delay line shaped signal is used to stop the TAC. The output of the TAC measures the range of the HI. The negative portion of the delay line shaped signal is also dE/dx. We do not present results of this last signal in this paper.

In Fig. 1 we pictorially describe the signals we use in BCS. Figure 1 shows the specific ionization as a function of position along the track of a stopping HI. The area under the curve is the total kinetic energy. The length of the curve determines the range of the HI. The Bragg peak is the maximum of the specific ionization. The dE/dx is the value of the specific ionization at the beginning of the track.

In Fig. 2 we show the experimental geometry used for testing this detector design. HI beams from both the 88" cyclotron and HILAC of LBL were used. Neon (5 MeV/amu), Argon (5 MeV/amu), Iron (8.5 MeV/amu), and Xenon (8.5 MeV/amu) beams impinged upon carbon and gold targets. Both elastically scattered particles and projectile fragments were used to probe the response of the detector.

III. Results and Discussion

The energy response of the detector was measured by elastically scattering 100 MeV Ne ions at 10 degrees from a .150 mg/cm^2 Au target. The detector had an angular acceptance of 0.003 radians. We measured a best energy resolution of 0.7% FWHM. Contributions to this resolution

from straggling in the target and detector window, from statistics, from kinematics and from the beam were estimated to be less than 0.25%. The screening inefficiency was calculated to be 0.2%. However, the value for the screening inefficiency implied from the Bragg peak energy dependence is about 4 times higher and possibly accounts for our measured energy resolution. Figure 3 shows a typical energy spectrum. The detector pressure was 300 torr for the Ne data.

A Bragg peak spectrum is shown in Fig. 4 for 100 MeV Ne ions. A resolution of 1.2% FWHM is measured. Calculating the energy straggling using Vavilov and assuming an effective charge of 7 we estimate a resolution of 1% FWHM at the Bragg peak.

The BCS range measurements as a function of energy is shown in Fig. 5. Note that the highest energy oxygen and carbon ions are passing through the counter at 300 torr. This range coincides with a distance of 28 cm. The lowest range observed was limited by the 3 cm grid to anode distance. A three dimensional view of this same data is shown in Fig. 6. Note that counts/channel is scaled logarithmically.

The BCS Bragg peak measurements as a function of range is shown in Fig. 7 and is from the same data set as shown in two previous figures. Note the oxygen and carbon ions that have ranges longer than the grid to cathode distance (28 cm) give Bragg peak signals which are too low but are easily identified in the range measurement. The merging of the Bragg peak signals at the lowest range is for particles whose range is less than or equal to the grid to anode distance (3 cm). Note that the Bragg peak signal is measuring the Z of the particle unambiguously. The slight slope in the Bragg peak response as a function of range is

believed to be due to the screening inefficiency and is an energy dependent correction. Figure 8 shows a three dimensional plot of these same data. If one accepts with a gate those particles having ranges between 3 cm and 28 cm in this detector and corrects the Bragg peak signal for the screening inefficiency we observe the Bragg peak spectrum shown in Fig. 9. This signal appears to be linear in Z to within 7%. The projected charge resolution in this spectrum is $\Delta Z = 0.16$ FWHM at a $Z = 10$.

In order to study the response of the BCS detector at higher atomic numbers we scattered 8.5 MeV/amu ^{56}Fe from ^{197}Au near the grazing angle (54°). For these data the detector was operated at a pressure of 270 torr and 100 V/cm electric field between cathode and grid. Instantaneous counting rates of between 10^3 and 10^4 events/s were used in taking the data.

The BCS energy/range signal should scale approximately as the atomic number, Z. Figure 10 shows a BCS energy/range spectrum in the mass 56 region. The charge resolution is sufficient to identify the elements near $Z = 26$. These data along with Bragg peak data yield a redundancy in the Z measurement. For this reason we study the Bragg peak as a function of energy/range for each event. Figure 11 shows a three dimensional plot of the Bragg peak as a function of energy/range. Note the relatively clean separation between elements in this mass region. Figure 12 shows a logarithmic counts/channel scale of the same data. We show the contour plot of the same graph in fig. 13. Here it is important to note that the best charge resolution is obtained along an axis through the elements having $Z \leq 26$. These are primarily

projectile fragments having velocities near the projectile velocity whereas those fragments above Z = 26 have much lower velocities and the energy/range signal appears less sensitive in the Z measurement. In order to achieve better Z resolution we will take a weighted average of the Bragg peak signal and the energy/range signal. Using this technique we see that the resolution will improve for $Z \leq 26$ and will become worst for $Z > 26$.

Figure 14 shows the Bragg peak spectra (no gates) and the effect of both the screening correction on the elemental resolving power and the effect of a weighted average signal optimizing the charge resolution. The peak to valley ratios of the Bragg peak spectra are clearly enhanced using these two corrections.

The same data are seen in Fig. 15 with an event gate turned on. This gate consists of requiring that the range X Bragg peak/energy be approximately a constant value. This removes particles outside the range limits of 3 and 28 cm. It also removes to some extent reactions in the detector.

An additional energy gate accepting only deep inelastic events yields the Bragg peak spectra shown in Fig. 16. Note that peak to valley ratios of 50:1 are observed between the elements in the mass 56 region. We measure a best charge resolution of 1.4% FWHM at charge of 26. This is to be compared with a calculated value of 0.6% FWHM using Vavalov energy straggling theory and an effective charge of 18. The linearity of the charge measurements is within 7% in this mass region.

IV. Summary

The Bragg Curvey Spectroscopy concept has been demonstrated to yield energy and charge measurements having resolutions of 0.7% and 1.2-1.4% FWHM respectively for heavy ions lighter than cobalt. The Bragg peak signal is seen to measure the charge unambiguously and would lend itself to the possibility of a fast charge gate. The Bragg peak signal appears to be linear in charge to within 7% for $Z \leq 26$.

Some of the problems to be solved in future work are as follows: What is the response of HI having $Z > 26$? What sort of mass resolution can the BCS concept achieve? What is the response to HI having energy less than 1 MeV/amu? Can the straggling be minimized in the Bragg curve by selecting a more appropriate ionization chamber medium?

Acknowledgements

This work has been done in collaboration with M. Bini, R. DeVries, R. Legrain, R. Loveman, W. Pang, Y.C. Peng, M. Roach, D.K. Scott, A. Shotter, W. Sondheim, T.J. Symons, J. Wouters, and M. Zisman and will appear in more detail in a subsequent publication.

This work was supported by the Director, Office of Energy Research, Division of Nuclear Physics of the Office of High Energy and Nuclear Physics and by Nuclear Sciences of the Basic Energy Sciences Program of the U.S. Department of Energy under Contract W-7405-ENG-48.

Table I

Design Parameters for BCS Detector

Cathode to grid distance	28 cm
Grid to anode distance	3 cm
Grid wire diameter	40 μm
wire spacing	560 μm
Electric field ratio (grid to anode: grid to cathode)	2.5
Cathode window, aluminized hostaphan	
Voltage divider pitch	2 cm^{-1}

Gas: 93% Ar + 7% CH_4

Figure Captions

Fig. 1. Bragg Curve Spectroscopy signals.

Fig. 2. The geometry used in testing the Bragg Curve Spectroscopy concept.

Fig. 3. BCS energy spectrum.

Fig. 4. BCS Bragg peak spectrum

Fig. 5. Two dimensional contour plot of correlation between BCS signals, range vs. energy. Mass 20 region.

Fig. 6. Three dimensional plot of correlations between BCS signals, range vs. energy vs. logarithm of counts. Mass 20 region.

Fig. 7. Two dimensional contour plot of correlations between BCS signals, Bragg peak vs. range. Mass 20 region.

Fig. 8. Three dimensional plot of correlations between BCS signals, Bragg peak vs. range vs. logarithm of counts. Mass 20 region.

Fig. 9. BCS Bragg peak spectrum, corrected for screening inefficiency. Mass 20 region. Range gate accepts events stopping between 2.1 and 19.6 mg/cm^2.

Fig. 10. BCS energy/range spectrum. Mass 56 region.

Fig. 11. Three dimensional plot of correlations between BCS signals, Bragg peak vs. energy/range vs. counts. Mass 56 region.

Fig. 12. Three dimensional plot of correlations between BCS signals, Bragg peak vs. energy/range vs. logarithm of counts. Mass 56 region

Fig. 13. Two dimensional contour plot of correlations between BCS signals, Bragg peak vs. energy/range. Mass 56 region. Contours biased to favor low counts.

Fig. 14. BCS Bragg peak spectra showing effects of screening in efficiency and energy/range averaging corrections. No gates. Mass 56 region.

Fig. 15. BCS Bragg peak spectra showing effects of screening in efficiency and energy/range averaging corrections. Event gate is on. Mass 56 region.

Fig. 16. BCS Bragg peak spectra showing effects of screening inefficiency and energy/range averaging corrections. Deep inelastic gate is on. Mass 56 region.

BRAGG CURVE SPECTROSCOPY

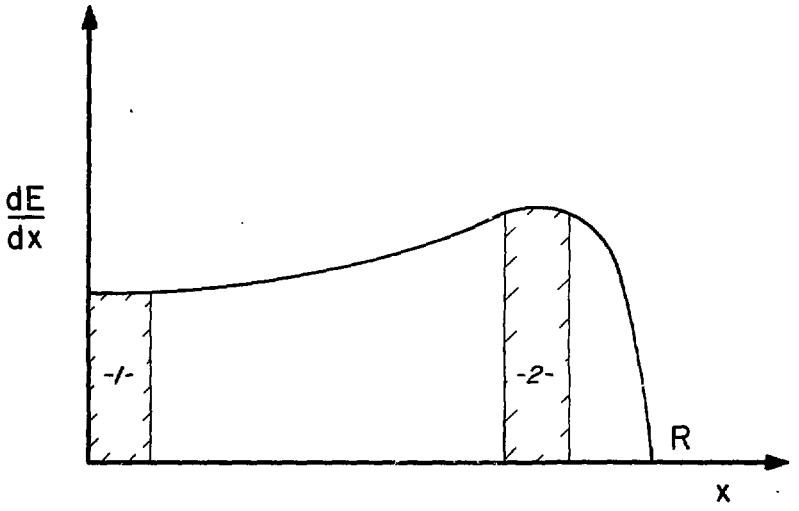

Area = Total kinetic energy (A,β)

Length = Range (A,Z,β)

$\frac{dE}{dx}(Z,\beta)$ [-1-]

Bragg Peak (Z) [-2-]

XBL 813-8715

Fig. 1

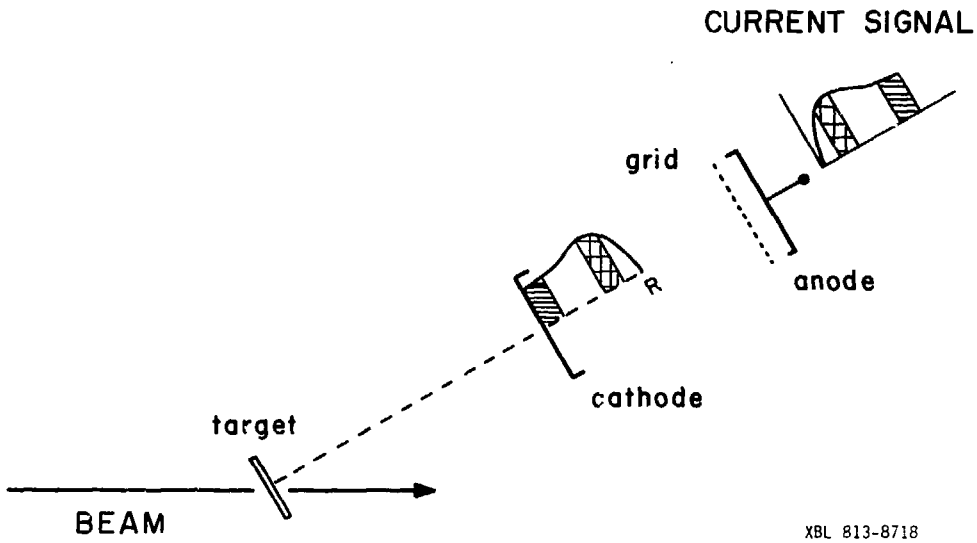
CURRENT SIGNAL
grid
anode
α
cathode
target
BEAM
XBL 813-8718

Fig. 2

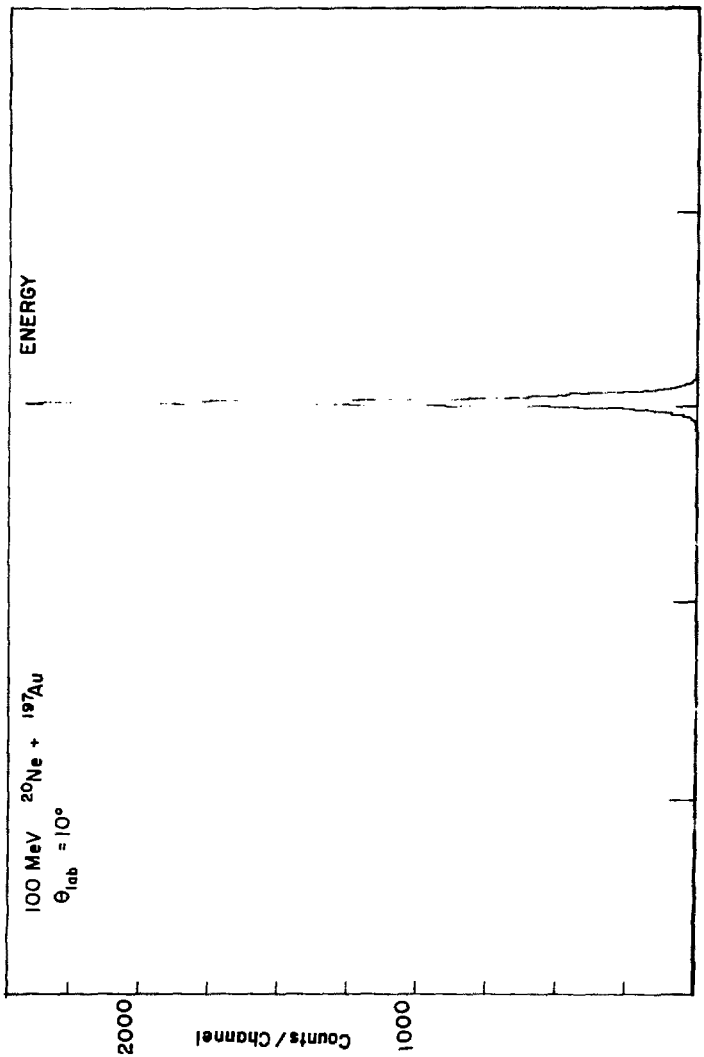

XBL 813-8672

Fig. 3

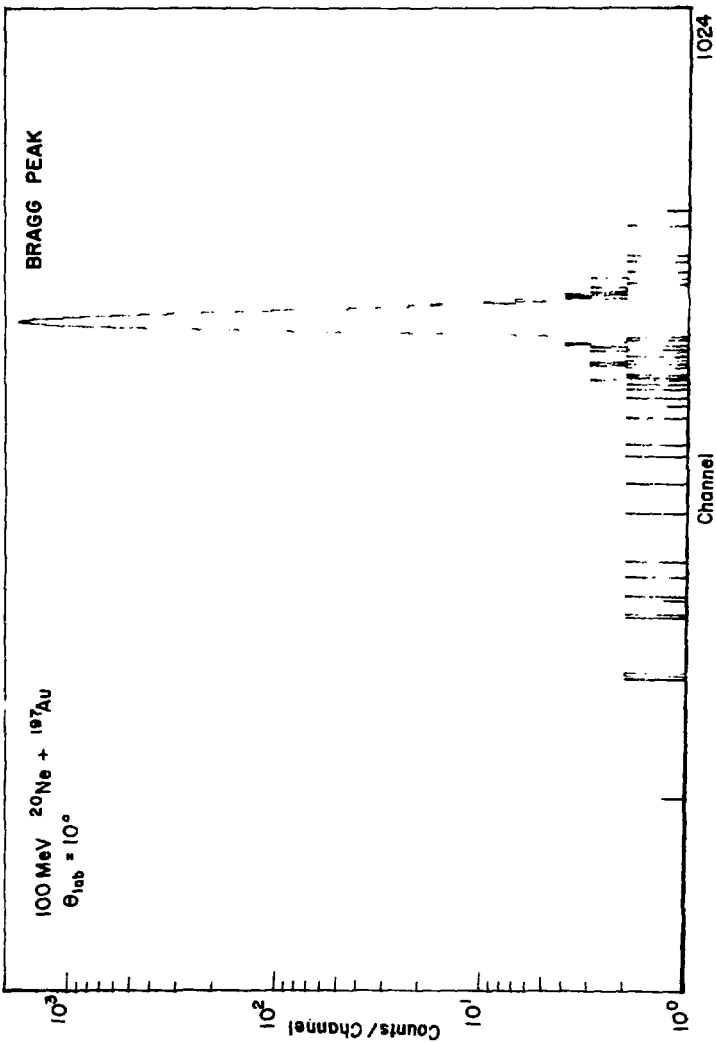

X8L 813-8673

Fig. 4

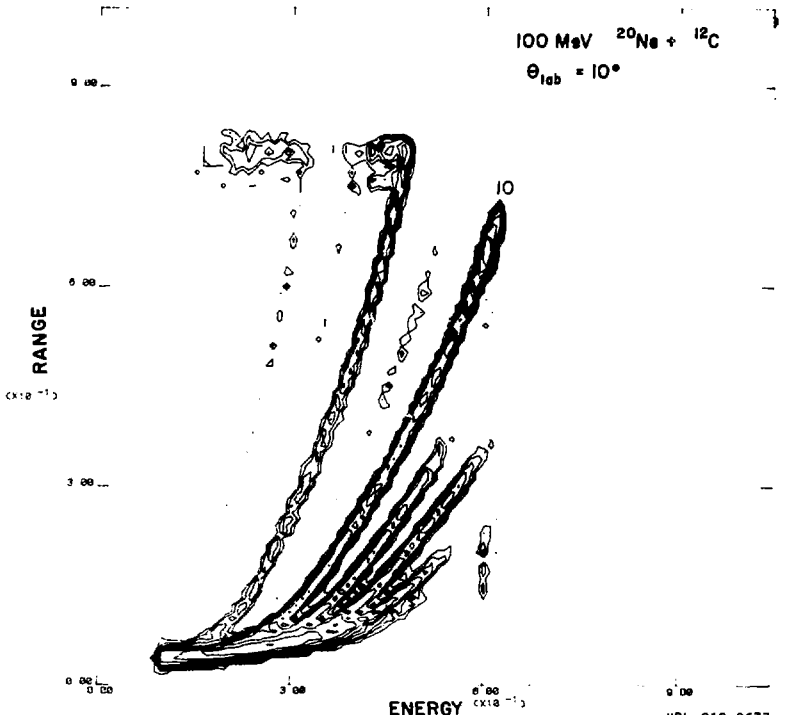

Fig. 5

100 MeV $^{20}Ne + {}^{12}C$

$\theta_{lab} = 10°$

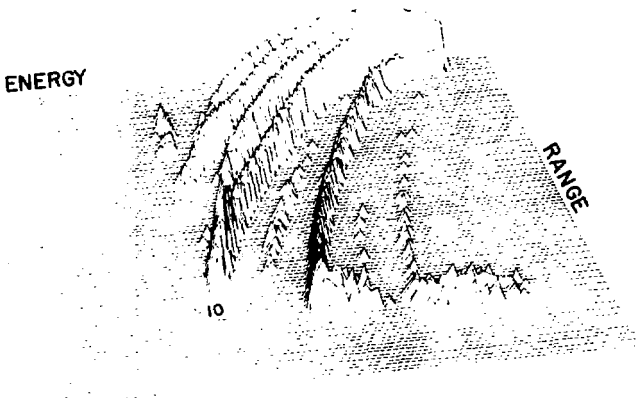

XBL 813-8676

Fig. 6

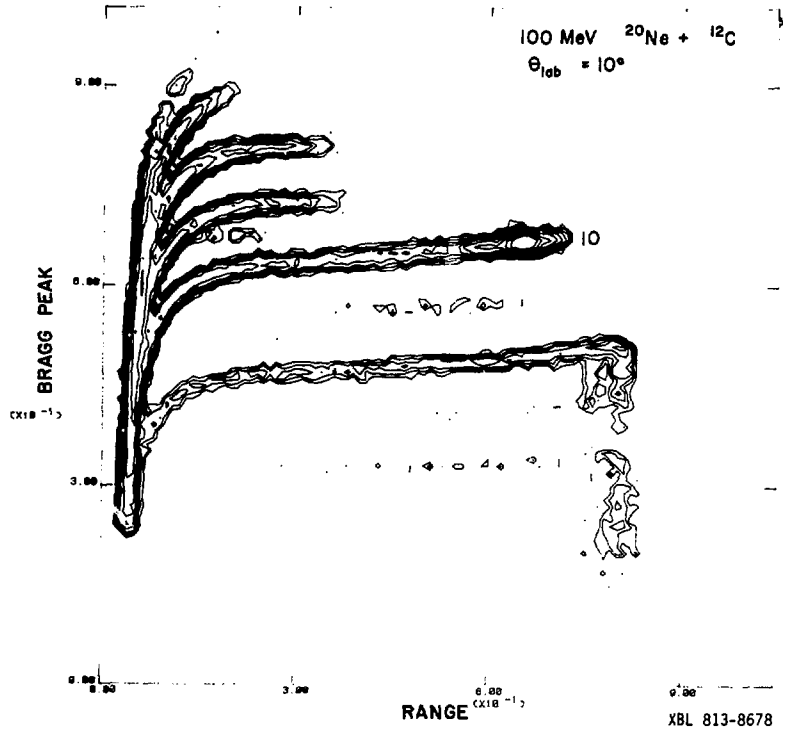
100 MeV ^{20}Ne + ^{12}C
θ_{lab} = 10°
10
BRAGG PEAK
(x10 $^{-1}$)
RANGE
(x10 $^{-1}$)
XBL 813-8678

Fig. 7

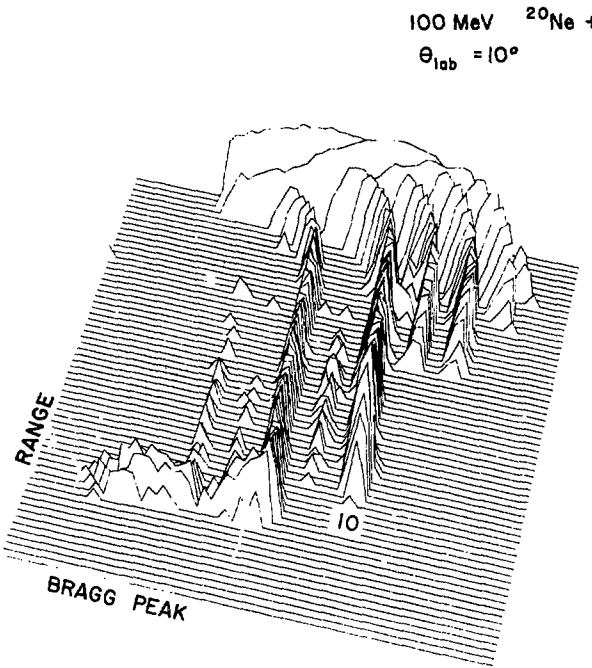

XBL 813-8675

Fig. 8

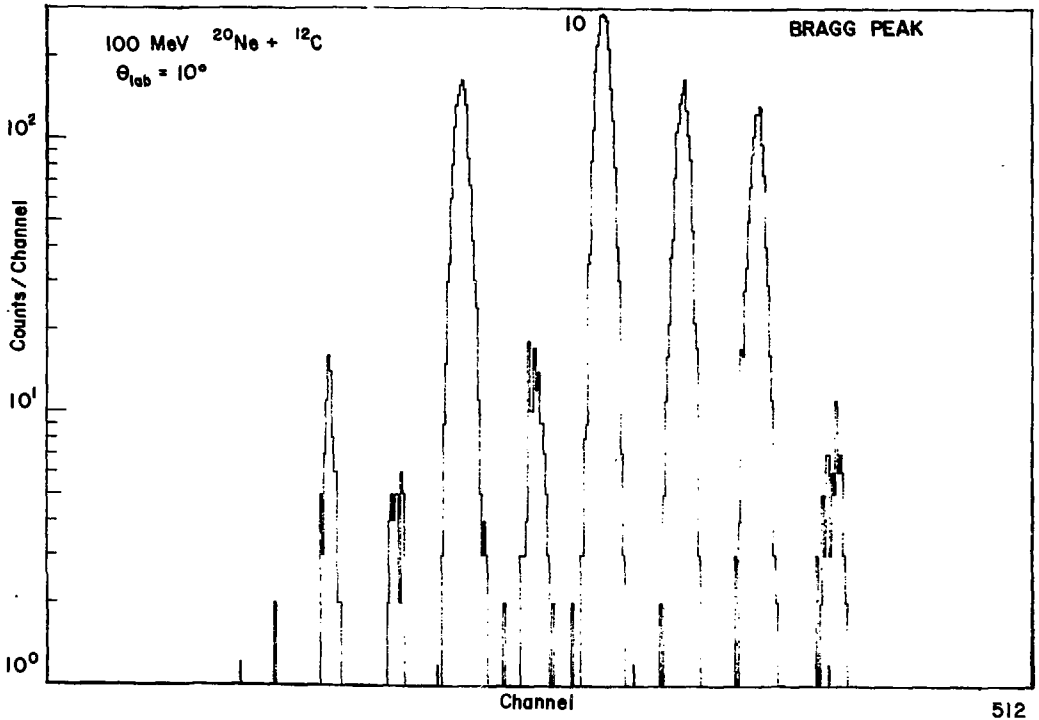

XBL 813-8671

Fig. 9

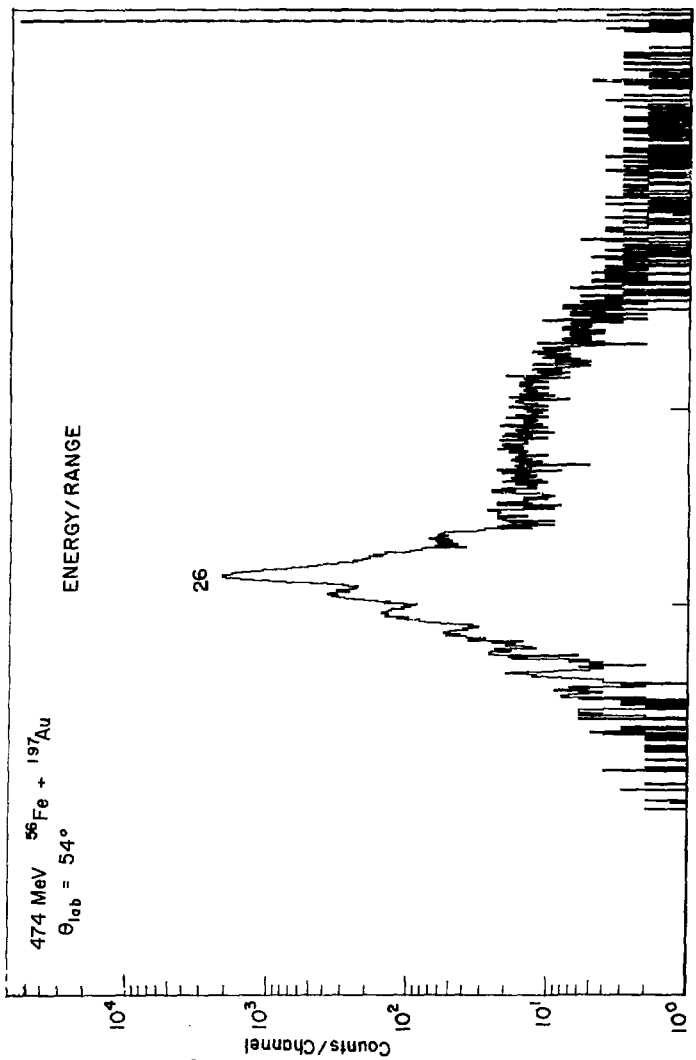
474 MeV ^{56}Fe + ^{197}Au
θ_{lab} = 54°
ENERGY/RANGE
26
Counts/Channel
10^4
10^3
10^2
10^1
10^0
Channel
1024
XBL 813-8679

Fig. 10

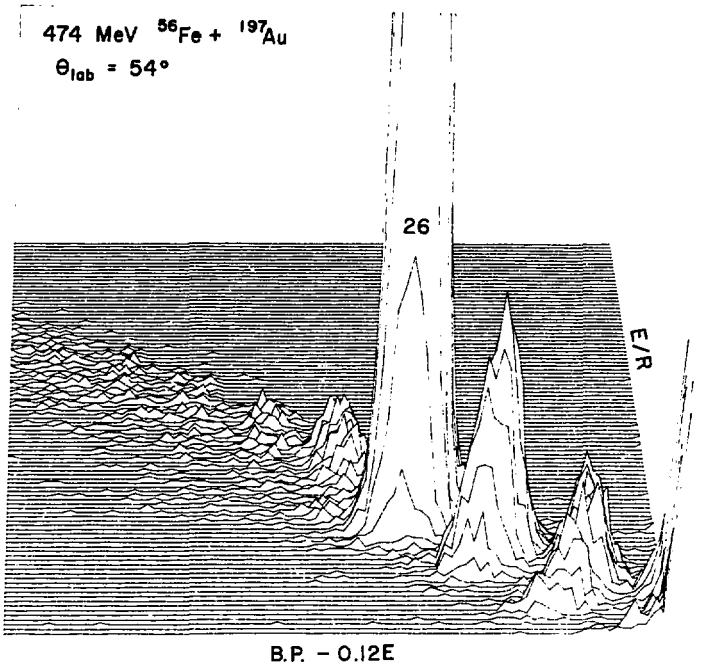

XBL 813-8667

Fig. 11

474 MeV $^{56}Fe + {}^{197}Au$
$\theta_{lab} = 54°$

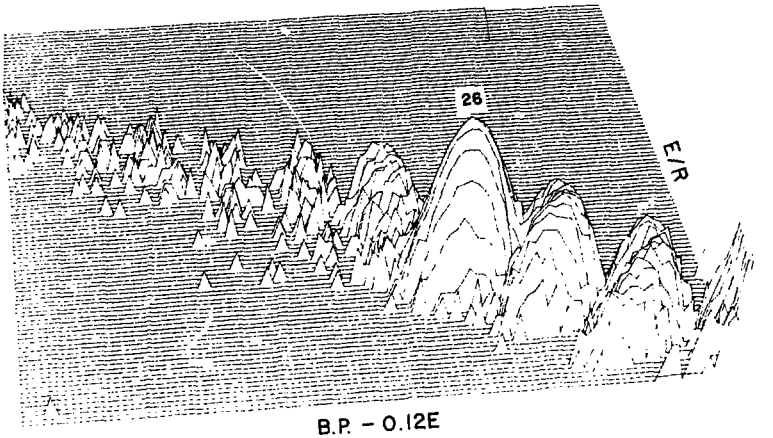

XBL 813-8668

Fig. 12

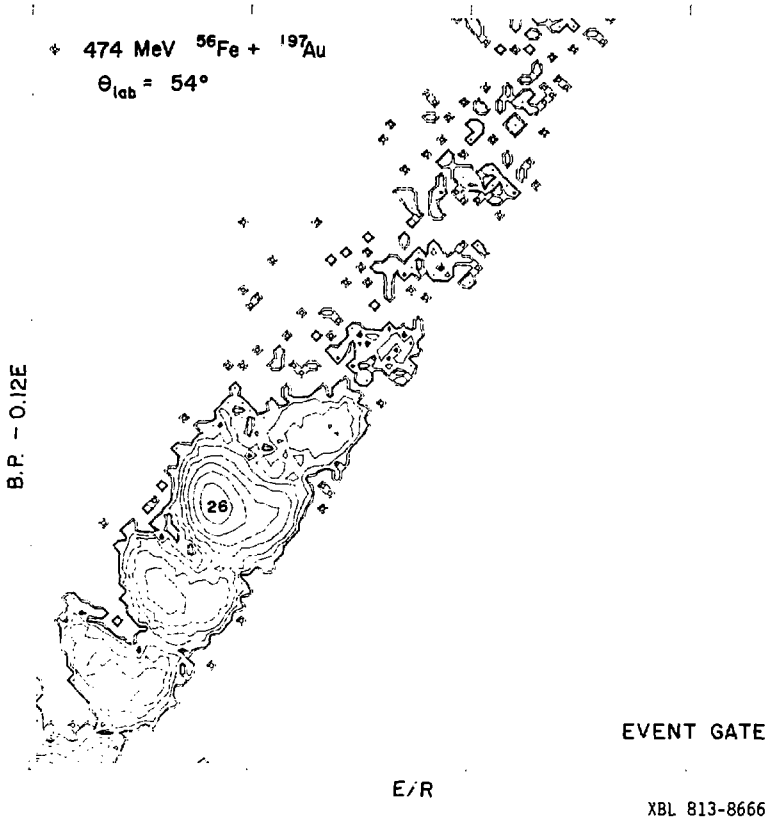
474 MeV ^{56}Fe + ^{197}Au
θ_{lab} = 54°
B.P. - 0.12E
26
EVENT GATE
E/R
XBL 813-8666

Fig. 13

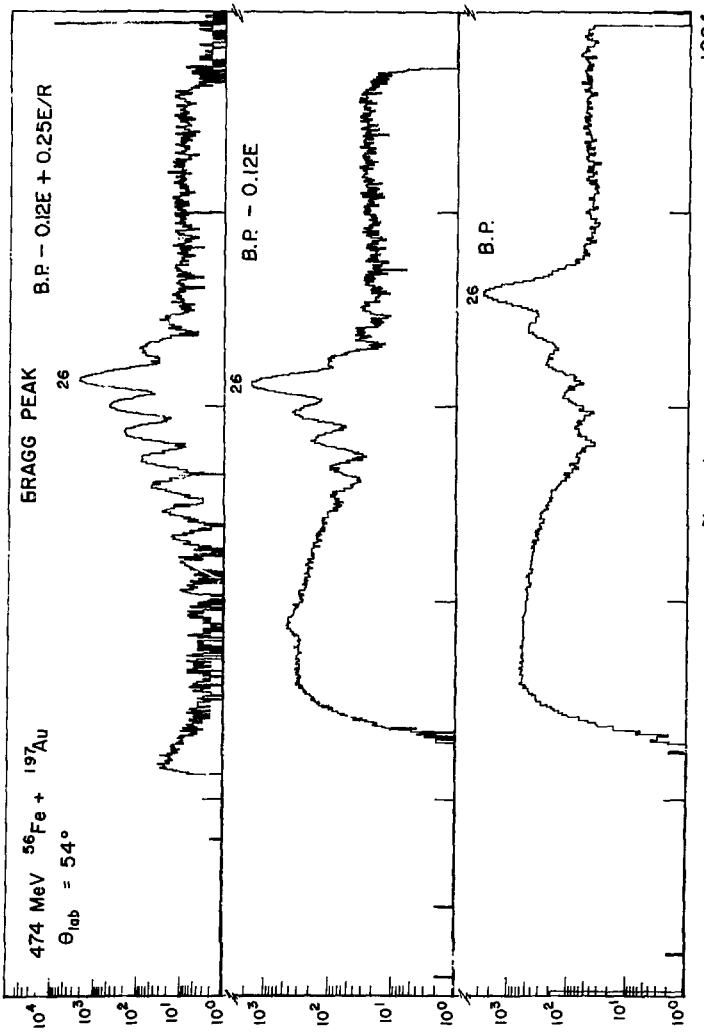

XBL 813-8674

Fig. 14

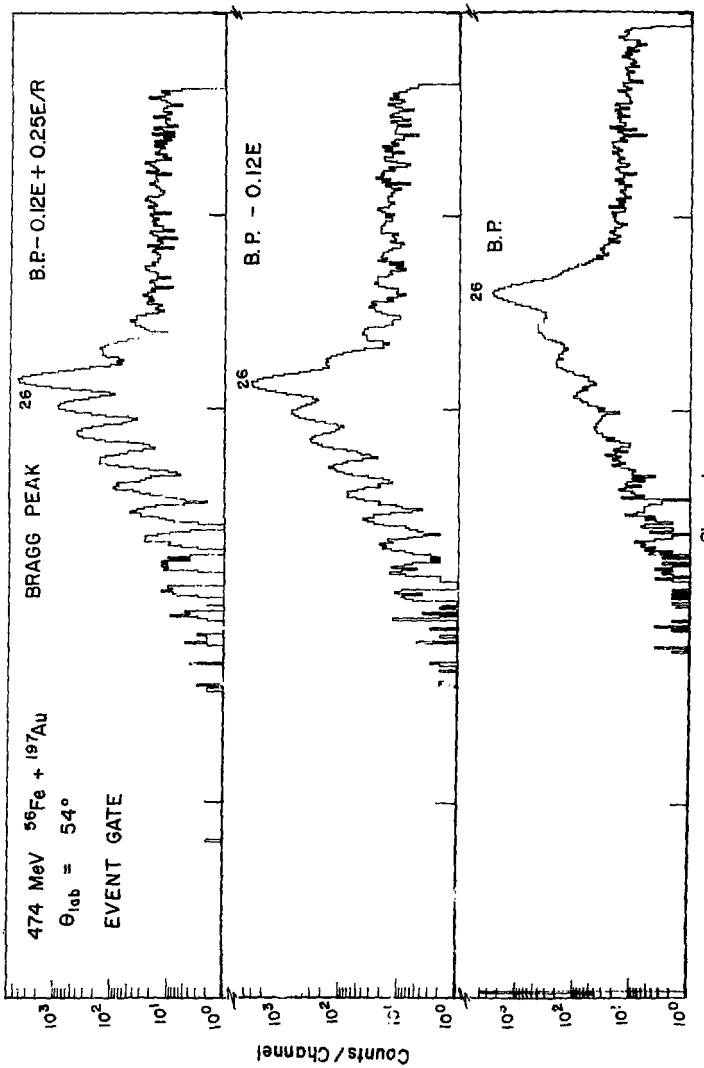
474 MeV 56Fe + 197Au
θlab = 54°
EVENT GATE
BRAGG PEAK
26
B.P.- 0.12E + 0.25E/R
B.P. - 0.12E
B.P.
Counts / Channel
Channel
512
XBL 813-8680

Fig. 15

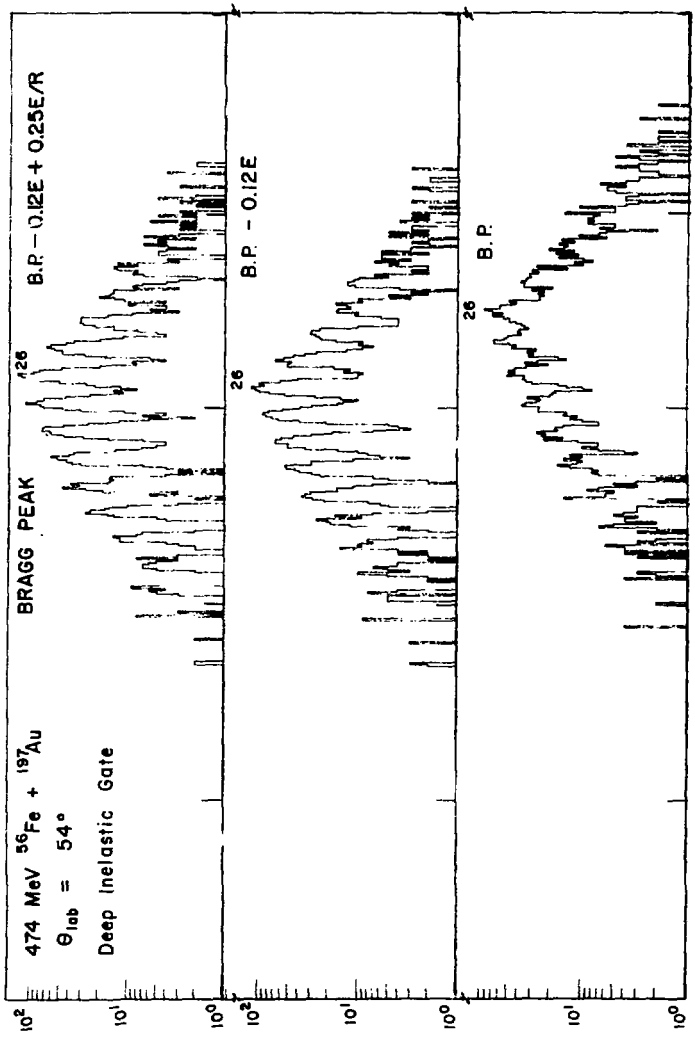

XBL 813-8669

Fig. 16